arXiv:1609.07024v1 [hep-ph] 22 Sep 2016

Spin effects in the pion holographic light-front wavefunction

Mohammad Ahmady*

Department of Physics, Mount Allison University,

Sackville, New Brunswick, Canada, E4L 1E6

Farrukh Chishtie†

Theoretical Research Institute, Pakistan Academy of

Sciences (TRIPAS), Islamabad 44000, Pakistan.

Ruben Sandapen‡

Department of Physics, Acadia University,

Wolfville, Nova-Scotia, Canada, B4P 2R6 and

Department of Physics, Mount Allison University,

Sackville, New Brunswick, Canada, E4L 1E6

Abstract

We account for dynamical spin effects in the holographic light-front wavefunction of the pion in order to predict the mean charge radius, $\sqrt{\langle r_\pi^2 \rangle}$, the decay constant, f_π, the spacelike electromagnetic form factor, $F_\pi(Q^2)$, the twist-2 pion Distribution Amplitude and the photon-to-pion transition form factor $F_{\gamma\pi}(Q^2)$. Using a universal fundamental AdS/QCD scale, $\kappa = 523$ MeV, and a constituent quark mass of 330 MeV, we find a remarkable improvement in describing all observables.

* mahmady@mta.ca

† fchishti@uwo.ca

‡ ruben.sandapen@acadiau.ca

I. INTRODUCTION

Hadronic light-front wavefunctions (LFWFs) provide the underlying link between the fundamental degrees of freedom of QCD, i.e. quarks and gluons, and their asymptotic hadronic states. LFWFs thus encode both the physics of confinement and chiral symmetry breaking, which are fundamental, intimately related [1] and yet not fully understood, emergent properties of QCD. In phenomenology, LFWFs are extremely important since all hadronic properties can, in principle, be derived from them. For example, in the exclusive decays of the B meson to light mesons, which are under intense investigation at the LHCb experiment, the theoretical non-perturbative inputs, i.e. the meson decay constants, Distribution Amplitudes and transition form factors can all be computed if the LFWFs of the mesons are known. These non-perturbative inputs are in fact the major source of theoretical uncertainties in current Standard Model predictions [2].

In principle, LFWFs are obtained by solving the LF Heisenberg equation for QCD: [3]

$$H_{\rm QCD}^{\rm LF}|\Psi(P)\rangle = M^2|\Psi(P)\rangle \tag{1}$$

where $H_{\rm QCD}^{\rm LF} = P^+P^- - P_\perp^2$ is the LF QCD Hamiltonian and M is the hadron mass. At equal light-front time ($x^+ = 0$) and in the light-front gauge $A^+ = 0$, the hadron state $|\Psi(P)\rangle$ admits a Fock expansion, i.e.

$$|\Psi(P^+, \mathbf{P}_\perp, S_z)\rangle = \sum_{n,h_i} \int [dx_i][d^2\mathbf{k}_{\perp i}] \frac{1}{\sqrt{x_i}} \Psi_n(x_i, \mathbf{k}_{\perp i}, h_i)|n : x_i P^+, x_i \mathbf{P}_\perp + \mathbf{k}_{\perp i}, h_i\rangle \tag{2}$$

where $\Psi_n(x_i, \mathbf{k}_{\perp i}, h_i)$ is the LFWF of the Fock state with n constituents and the integration measures are given by

$$[dx_i] \equiv \prod_i^n {\rm d}x_i \delta(1 - \sum_{j=1}^n x_j) \qquad [{\rm d}^2\mathbf{k}_i] \equiv \prod_{i=1}^n \frac{{\rm d}^2\mathbf{k}_i}{2(2\pi)^3} 16\pi^3 \delta^2(\sum_{j=1}^n \mathbf{k}_i)\ . \tag{3}$$

LFWFs are quantum mechanical probability amplitudes that depends on the momenta fraction $x_i = k_i^+/P^+$, the transverse momenta $\mathbf{k}_{\perp i}$, and the helicities h_i of the constituents. In practice, it is difficult, if not impossible, to solve Eq. (1) since it contains an infinite number of strongly coupled integral equations. Various approximation schemes involve truncating the Fock expansion, using discretized light-front quantization or solving the equations in a lower number of spatial dimensions. For a review of light-front quantum field theories, we refer to [4].

A remarkable breakthrough during the last decade is the discovery by Brodsky and de Téramond [5–8] of a higher dimensional gravity dual to a semiclassical approximation of light-front QCD. The result is a relativistic Schrödinger-like wave equation for mesons that can be solved analytically to predict meson spectroscopy and LFWFs in terms of a single mass scale κ. The approach can also include baryons [7] and more recently has been extended to a unified framework for baryons and mesons considered as conformal superpartners [9]. This gauge/gravity duality is referred to as light-front holography (LFH) and is reviewed in Ref. [3].

In the semiclassical approximation, quark masses and quantum loops are neglected, the LFWFs depend on the invariant mass $\mathcal{M}^2 = (\sum_i^n k_i)^2$ of the constituents rather than on their individual momenta k_i. For the valence ($n = 2$ for mesons) Fock state, the invariant mass of the $q\bar{q}$ pair is $\mathcal{M}^2_{q\bar{q}} = k_\perp^2/x(1-x)$ and the latter is the Fourier conjugate to the impact variable $\zeta^2 = x(1-x)b^2$ where b is the transverse separation the quark and antiquark. The valence meson LFWF can then be written in a factorized form:

$$\Psi(\zeta, x, \phi) = e^{iL\phi}\mathcal{X}(x)\frac{\phi(\zeta)}{\sqrt{2\pi\zeta}} \tag{4}$$

where the helicity indices have been suppressed [3]. We note that this suppression of the helicity indices is legitimate if either the constituents are assumed to be spinless or if the helicity dependence decouples from the dynamics. It can then be shown that Eq. (1) reduces to a 1-dimensional Schrödinger-like wave equation for the transverse mode of LFWF of the valence ($n = 2$ for mesons) state, namely:

$$\left(-\frac{d^2}{d\zeta^2} - \frac{1-4L^2}{4\zeta^2} + U(\zeta)\right)\phi(\zeta) = M^2\phi(\zeta) \tag{5}$$

where all the interaction terms and the effects of higher Fock states on the valence state are hidden in the confinement potential $U(\zeta)$. The latter remains to be specified and, at present, this cannot be done from first principles in QCD.

However, Brodsky and de Téramond found that Eq. (5) maps onto the wave equation for the propagation of spin-J string modes in the higher dimensional anti-de Sitter space, AdS_5, if the impact light-front variable ζ is identified with z_5, the fifth dimension of AdS space and the light-front orbital angular momentum L^2 is mapped onto $(mR)^2 - (2-J)^2$ where R and m are the AdS radius and mass respectively. For this reason, we refer to Eq. (5) as the holographic LF Schrödinger equation. In this AdS/QCD duality, the confining potential

in physical spacetime is driven by the deformation of the pure AdS_5 geometry. Specifically, the potential is given by

$$U(z_5, J) = \frac{1}{2}\varphi''(z_5) + \frac{1}{4}\varphi'(z_5)^2 + \left(\frac{2J-3}{4z_5}\right)\varphi'(z_5) \tag{6}$$

where $\varphi(z_5)$ is the dilaton field which breaks conformal invariance in AdS space. A quadratic dilaton, $\varphi(z_5) = \kappa^2 z_5^2$, profile results in a light-front harmonic oscillator potential in physical spacetime:

$$U(\zeta, J) = \kappa^4\zeta^2 + \kappa^2(J-1) \tag{7}$$

since z_5 maps onto the LF impact variable ζ. Remarkably, Brodsky, Dosch and de Téramond have shown that the quadratic form of the AdS/QCD potential is unique [10]. In fact, starting with a more general dilaton profile $\varphi \propto z_5^s$ and requiring the pion to be massless, uniquely fixes $s = 2$ [11]. More formally, applying the mechanism of de Alfaro, Furbini and Furlan [12] (which allows the emergence of a mass scale in the Hamiltonian of a conformal 1-dimensional QFT while retaining the conformal invariance of the underlying action) to semiclassical LF QCD uniquely fixes the quadratic form of the AdS/QCD potential [10].

With the confining potential specified, one can solve the holographic Schrödinger equation to obtain the meson mass spectrum,

$$M^2 = 4\kappa^2\left(n + L + \frac{S}{2}\right) \tag{8}$$

which, as expected, predicts a massless pion. The corresponding normalized eigenfunctions are given by

$$\phi_{nL}(\zeta) = \kappa^{1+L}\sqrt{\frac{2n!}{(n+L)!}}\zeta^{1/2+L}\exp\left(\frac{-\kappa^2\zeta^2}{2}\right)L_n^L(x^2\zeta^2)\ . \tag{9}$$

To completely specify the holographic meson wavefunction, we need the analytic form of the longitudinal mode $\mathcal{X}(x)$. This is obtained by matching the expressions for the pion EM or gravitational form factor in physical spacetime and in AdS space. Either matching consistently results in $\mathcal{X}(x) = \sqrt{x(1-x)}$ [5, 13]. The meson holographic LFWFs for massless quarks can thus be written in closed form:

$$\Psi_{nL}(\zeta, x, \phi) = e^{iL\phi}\sqrt{x(1-x)}(2\pi)^{-1/2}\kappa^{1+L}\sqrt{\frac{2n!}{(n+L)!}}\zeta^L\exp\left(\frac{-\kappa^2\zeta^2}{2}\right)L_n^L(x^2\zeta^2) \tag{10}$$

with the corresponding meson masses lying on linear Regge trajectories as given by Eq. (8). The reasons why a solution to a quantum field theory could reduce to a solution of a simple, one-dimensional differential equation are explored in Ref. [14].

For phenomenological applications, it is necessary to restore both the quark mass and helicity dependence of the holographic LFWF. In fact, it has recently been shown in Ref. [15] that non-zero light quark masses drastically improves the description of data on the photon-to-pion, photon-to-η and photon-to-η' transition form factors. On the other hand, for the pion and kaon EM form factors, the description of data actually worsens unless 3 data points at large Q^2 are excluded for the kaon form factor [15]. Accounting for non-zero light quark masses means going beyond the semiclassical approximation, and this is usually done following the prescription of Brodsky and de Téramond [16]. For the ground state pion, this leads to

$$\Psi^{\pi}(x,\zeta) = \mathcal{N}\sqrt{x(1-x)}\exp\left[-\frac{\kappa^2\zeta^2}{2}\right]\exp\left[-\frac{m_f^2}{2\kappa^2 x(1-x)}\right] \tag{11}$$

where $\mathcal{N}$ is a normalization constant fixed by requiring that

$$\int \mathrm{d}^2\mathbf{b}\mathrm{d}x|\Psi^{\pi}(x,\zeta)|^2 = P_{q\bar{q}} \tag{12}$$

where $P_{q\bar{q}}$ is the probability that the meson consists of the leading quark-antiquark Fock state.

Note Eq. (8) tells us that the AdS/QCD scale κ can be chosen to fit the experimentally measured Regge slopes. Ref. [3] reports $\kappa = 590$ MeV for pseudoscalar mesons and $\kappa = 540$ MeV for vector mesons. A recent fit to the Regge slopes of mesons and baryons, treated as conformal superpartners, yields $\kappa = 523$ MeV [9]. On the other hand, the AdS/QCD scale κ can be connected to the scheme-dependent pQCD renormalization scale $\Lambda_{\rm QCD}$ by matching the running strong coupling in the non-perturbative (described by light-front holography) and the perturbative regimes [17]. With $\kappa = 523$ MeV and the β-function of the QCD running coupling at 5-loops, Brodsky, Deur and de Téramond recently predicted the QCD renormalization scale, $\Lambda_{\rm QCD}^{\overline{MS}}$, in excellent agreement with the world average value [18]. Furthermore, light-front holographic wavefunctions have also been used to predict diffractive vector meson production[19, 20]. A fit to the HERA data on diffractive ρ electroproduction, with $m_{u/d} = 140$ MeV, gives $\kappa = 560$ MeV[19] and using $\kappa = 550$ MeV (with $m_{u/d}[m_s] = 46[140]$ MeV) leads to a good simultaneous description of the HERA data on diffractive ρ and ϕ electroproduction [20]. These findings hint towards the emergence of a universal fundamental AdS/QCD scale $\kappa \sim 550$ MeV. In the most recent application of LFH to predict nucleon EM form factors [21], it is pointed out that this universality holds

up to 10% accuracy. In this paper, we shall use the value of $\kappa = 523$ MeV which fits the meson/baryon Regge slopes and accurately predicts $\Lambda_{\rm QCD}^{\overline{MS}}$ [9, 18].

In earlier applications of LFH with massless quarks, much lower values of κ were required to fit the pion data: $\kappa = 375$ MeV in Ref. [8] in order to fit the pion EM form factor data and $\kappa = 432$ MeV (with $P_{q\bar{q}} = 0.5$) to fit the photon-to-pion transition form factor data simultaneously at large Q^2 and $Q^2 = 0$ (the latter is fixed by the $\pi^0 \to \gamma\gamma$ decay width) [22]. Note that in Ref. [8], the EM form factor is computed, both in the spacelike and timelike regions, as a convolution of normalizable hadronic modes with a non-normalizable EM current which propagates in the modified infrared region of AdS space and generates the non-perturbative pole structure of the EM form factor in the timelike region. Alternatively, the spacelike EM form factor can be computed using the Drell-Yan-West formula [23, 24] in physical spacetime with the holographic pion LFWF. The latter approach is taken in Refs. [15, 25–27]. In Ref. [15], with $m_{u/d} = 330$ MeV, the authors use a universal $\kappa = 550$ MeV for all mesons but fix the wavefunction normalization for the pion so as to fit the decay constant. Consequently, this implies that $P_{q\bar{q}} = 0.61$ only for the pion. In Ref. [26], a higher value of $\kappa = 787$ MeV is used with $m_{u/d} = 330$ MeV and the authors predict $P_{q\bar{q}} = 0.279$, implying an important contribution of higher Fock states in the pion. In Ref. [27], a universal AdS/QCD scale $\kappa = 550$ MeV is used for all mesons, together with a constituent quark mass $m_{u/d} = 420$ MeV, but $P_{q\bar{q}} = 0.6$ is fixed for the pion only: for the kaon, $P_{q\bar{q}} = 0.8$ and for all other mesons, $P_{q\bar{q}} = 1$.

All these previous studies seem to indicate that a special treatment is required at least for the pion either by using a distinct AdS/QCD scale κ or/and relaxing the normalization condition on the holographic wavefunction, i.e. invoking higher Fock states contributions. This may well be reasonable since the pion is indeed unnaturally light and does not lie on a Regge trajectory, as pointed out in Ref. [25]. However, we note that in the previous studies [15, 26, 27] where the pion observables are predicted using the holographic wavefunction, given by Eq. (11), the helicity dependence of the latter is always assumed to decouple from the dynamics, i.e. the helicity wavefunction is taken to be momentum-independent. This is actually consistent with the semi-classical approximation within which the AdS/QCD correspondence is exact. Consequently, Ref. [27] derives a single formula to predict simultaneously the vector and pseudoscalar meson decay constants, so that using a universal scale κ and $P_{q\bar{q}} = 1$ for all mesons inevitably leads to degenerate decay constants in conflict with

experiment.

In this paper, we show that it is possible to achieve a better description of the pion observables by using a universal AdS/QCD scale κ and without the need to invoke higher Fock state contributions. We do so by taking into account dynamical spin effects in the holographic pion wavefunction, i.e. we use a momentum-dependent helicity wavefunction. This approach goes beyond the semiclassical approximation, just like the inclusion of light quark masses in the holographic wavefunction. However, it does support the idea of the emergence of a universal, fundamental AdS/QCD scale. A similar approach was taken previously for the ρ meson, leading to impressive agreement to the HERA data on diffractive ρ electroproduction [19].

II. DYNAMICAL SPIN EFFECTS

To restore the helicity dependence of the holographic wavefunction, we assume that

$$\Psi(x,\mathbf{k}) \to \Psi_{h\bar{h}}(x,\mathbf{k}) = S_{h\bar{h}}(x,\mathbf{k})\Psi(x,\mathbf{k}) \tag{13}$$

where the helicity wavefunction $S_{h\bar{h}}(x,\mathbf{k})$ corresponds to the helicity wavefunction for a point-like meson-$q\bar{q}$ coupling. For vector mesons, the helicity wavefunction is therefore similar to that of the point-like photon-$q\bar{q}$ coupling, i.e.

$$S^V_{h\bar{h}}(x,\mathbf{k}) = \frac{\bar{v}_{\bar{h}}((1-x)P^+,-\mathbf{k})}{\sqrt{(1-x)}}[\gamma\cdot\epsilon_V]\frac{u_h(xP^+,\mathbf{k})}{\sqrt{x}} \tag{14}$$

where ϵ^μ_V is the polarization vector of the vector meson. Indeed, substituting ϵ^μ_V by the photon polarization vector and multiplying Eq. (14) by the light-front energy denominator [28] yields the well-known photon light-front wavefunctions [28–32]. This assumption for the helicity structure of the vector meson is very common when computing diffractive vector meson production in the dipole model [31–40] and, as we mentioned earlier, was used in Ref. [19] with the holographic wavefunction for the ρ meson.

For the pseudoscalar pion, the simplest approach is to replace $\gamma\cdot\epsilon_V$ in Eq. (14) by $iM_\pi\gamma^5$, i.e.

$$S^\pi_{h\bar{h}}(x,\mathbf{k}) = \frac{\bar{v}_{\bar{h}}((1-x)P^+,-\mathbf{k})}{\sqrt{1-x}}\left[iM_\pi\gamma^5\right]\frac{u_h(xP^+,\mathbf{k})}{\sqrt{x}}\,. \tag{15}$$

This minimal γ^5 structure is used in Refs. [41, 42] but other more general choices can be found in the literature [43, 44]. The factor i ensures the positive-definiteness of the LFWF

and the factor M_π implies that our wavefunction vanishes in the chiral limit which we do not consider in this paper. Evaluating the right-hand-side of Eq. (15) using the light-front spinors given in Ref. [28], we obtain

$$S^{\pi}_{h\bar{h}}(x,\mathbf{k}) = \frac{iM_\pi}{x(1-x)}(\bar{h}m_f\delta_{-h\bar{h}} + ke^{ih\theta_k}\delta_{h\bar{h}}) \tag{16}$$

where $\mathbf{k} = ke^{i\theta_k}$. Note that this helicity wavefunction allows configurations in which the quark and antiquark have same helicities. These configurations are expected to be present in the pion LFWF [45, 46]. In the non relativistic limit, $k \ll m_f$ and $x \approx 1/2$, only the configurations in which the quark and antiquark have opposite helicities survive, i.e.

$$S^{\pi}_{h\bar{h}}(x,\mathbf{k}) \to S^{\pi[\mathrm{nr}]}_{h\bar{h}} = \frac{i}{\sqrt{2}}\bar{h}\delta_{-h\bar{h}} \tag{17}$$

where we have normalized the helicity wavefunction such that $\sum_{h\bar{h}} |S^{\pi[\mathrm{nr}]}_{h,\bar{h}}|^2 = 1$. Eq. (17) is the helicity structure assumed for the meson (both pseudoscalar and vector) holographic wavefunction in Refs. [15, 26] and we shall refer to it as the non-relativistic helicity wavefunction.

Using Eq. (13) and Eq. (16), we can write down our spin-improved holographic pion wavefunction:

$$\Psi^{\pi}_{h\bar{h}}(x,\mathbf{k}) = iM_\pi\left[\bar{h}\delta_{-h\bar{h}}m_f + \delta_{h\bar{h}}ke^{ih\theta_k}\right]\frac{\Psi^\pi(x,\mathbf{k})}{x(1-x)} \tag{18}$$

which can be compared to the original holographic wavefunction, obtained using Eq. (13) and Eq. (17), i.e.

$$\Psi^{\pi[\mathrm{o}]}_{h\bar{h}}(x,\mathbf{k}) = \frac{i}{\sqrt{2}}\bar{h}\delta_{-h\bar{h}}\Psi^\pi(x,\mathbf{k})\ . \tag{19}$$

A two-dimensional Fourier transform of Eq. (18) and Eq. (19) to impact space gives

$$\Psi^{\pi}_{h\bar{h}}(x,\mathbf{b}) = iM_\pi\left[\bar{h}\delta_{-h\bar{h}}m_f - \delta_{h\bar{h}}ie^{ih\theta_b}\partial_b\right]\frac{\psi(x,\zeta)}{x(1-x)} \tag{20}$$

and

$$\Psi^{\pi[\mathrm{o}]}_{h\bar{h}}(x,\mathbf{b}) = \frac{i}{\sqrt{2}}\bar{h}\delta_{-h\bar{h}}\Psi(x,\zeta) \tag{21}$$

respectively.

We now fix the normalization constant $\mathcal{N}$ appearing in Eq. (4) by requiring that

$$\int \mathrm{d}^2\mathbf{b}\mathrm{d}x|\Psi^\pi(x,\mathbf{b})|^2 = 1 \tag{22}$$

where

$$|\Psi^{\pi}(x,\mathbf{b})|^2 \equiv \sum_{h,\bar{h}} |\Psi^{\pi}_{h\bar{h}}(x,\mathbf{b})|^2 \ . \tag{23}$$

Note that Eq. (22) reduces to the normalization condition given by Eq. (12) (with $P_{q\bar{q}} = 1$) if we substitute the original holographic wavefunction, Eq. (21), in Eq. (22). Imposing our normalization condition, Eq. (22), implies that we assume that the pion consists only of the leading quark-antiquark Fock state.

In Figures 1 and 2, we show the dynamical spin effects in the holographic wavefunction squared, after summing over all helicities. As can be clearly seen, the effect is a broadening of the wavefunction, i.e. a smooth enhancement of the end-point contributions.

III. EM FORM FACTOR AND RADIUS

Having specified the pion holographic LFWF, we are now in a position to compute several pion observables. We start with the EM form factor defined as

$$\langle \pi^+ : P' | J^{\mu}_{\rm em}(0) | \pi^+ : P \rangle = 2(P+P')^{\mu} F_{\pi}(Q^2) \tag{24}$$

where $P' = P + q$, $Q^2 = -q^2$ and the EM current $J^{\mu}_{\rm em}(z) = \sum_f e_f \bar{\Psi}(z)\gamma^{\mu}\Psi(z)$ with $f = \bar{d}, u$ and $e_{\bar{d},u} = 1/3, 2/3$. The EM form factor can be expressed in terms of the pion LFWF using the Drell-Yan-West formula [23, 24]:

$$F_{\pi}(Q^2) = 2\pi \int {\rm d}x{\rm d}b \ b \ J_0[(1-x)bQ] \ |\Psi^{\pi}(x,\mathbf{b})|^2 \tag{25}$$

where $|\Psi^{\pi}(x,\mathbf{b})|^2$ is given by Eq. (23). Note that Eq. (25) implies that $F_{\pi}(0) = 1$ if the pion LFWF is normalized according to Eq. (22).

Our predictions for the EM form factor using the original (dashed-blue curve) and our spin-improved (continuous-red curve) are compared with the data from CERN [47], CEA [48], Cornell [49–51], Jlab [52, 53] and CLEO [54, 55]. As can be seen, the agreement with data is very much improved with our spin-improved holographic wavefunction. In fact, we achieve excellent agreement with data from the lowest Q^2 datum to $Q^2 \approx 7$ GeV^2. For $Q^2 > 7\,{\rm GeV}^2$, our predictions with the original and spin-improved holographic wavefunctions coincide and they both undershoot the precise CLEO data [54]. This is the short-distance regime where perturbative corrections, not taken into account in the purely non-perturbative holographic wavefunction, become important. It is worth highlighting that agreement with

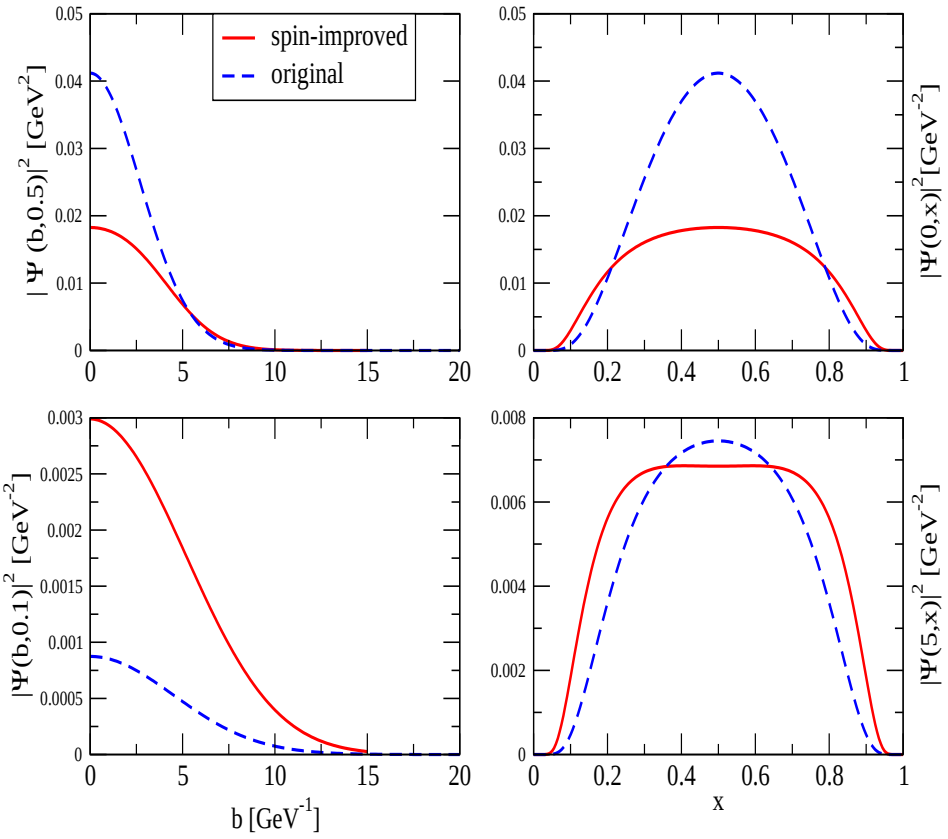

FIG. 1. The pion holographic LFWF squared and summed over all helicities: , $|\Psi^\pi(x,\mathbf{b})|^2$ [GeV^2]. Continuous-red curves: spin-improved wavefunction. Dashed-blue curves: original wavefunction. Left: The b-dependence of the wavefunction at fixed $x = 0.5$ (upper) and $x = 0.1$ (lower). Right: The x-dependence of the wavefunction at fixed $b = 0$ (upper) and $b = 5$ GeV^{-1} (lower). All plots are generated with $\kappa = 523$ GeV and $m_f = 330$ MeV.

the precise data in the non-perturbative region, $Q^2 \leq 1$ GeV^2, is excellent with our spin-improved holographic wavefunction.

The slope of the EM form factor at $Q^2 = 0$ is related to the mean radius of the pion [8]:

$$\langle r_\pi^2 \rangle = -\frac{6}{F_\pi(0)} \frac{\mathrm{d}F_\pi}{\mathrm{d}Q^2}\bigg|_{Q^2=0} \tag{26}$$

FIG. 2. The normalized pion holographic wavefunction squared and summed over helicities: $|\Psi^\pi(x,\mathbf{b})|^2$ [GeV^2], as a function of the transverse separation b [GeV^{-1}] and momentum fraction x. Left: original wavefunction. Right: spin-improved wavefunction. Both plots are generated with $\kappa = 523$ MeV and $m_f = 330$ MeV.

so that, using Eq. (25), we have

$$\sqrt{\langle r_\pi^2\rangle} = \left[\frac{3}{2}\int \mathrm{d}x\mathrm{d}^2\mathbf{b}[b(1-x)]^2|\Psi^\pi(x,\mathbf{b})|^2\right]^{1/2} . \tag{27}$$

Our predictions for the pion radius are compared to the measured value in Table I. As can be seen, we achieve a much better agreement with our spin-improved holographic wavefunction, reducing the percentage difference between the theory prediction and the central measured value from 19% to 2%.

Note that if we compute the pion radius using the original holographic wavefunction but with $\kappa = 540$ MeV and $m_f = 330$ MeV as in Ref. [15], we obtain $\sqrt{\langle r_\pi^2\rangle} = 0.530$ fm which is to be compared with the prediction of Ref. [15]: $\sqrt{\langle r_\pi^2\rangle} = 0.529$ fm. In Ref. [15], the authors obtain the pion radius from the slope of the EM pion form factor $F_\pi(Q^2)$ at $Q^2 = 0$ with the constraint that $F(0) = 1$. We note that the latter constraint on the form factor is automatically satisfied if the pion wavefunction is normalized with $P_{q\bar{q}} = 1$. Thus, although

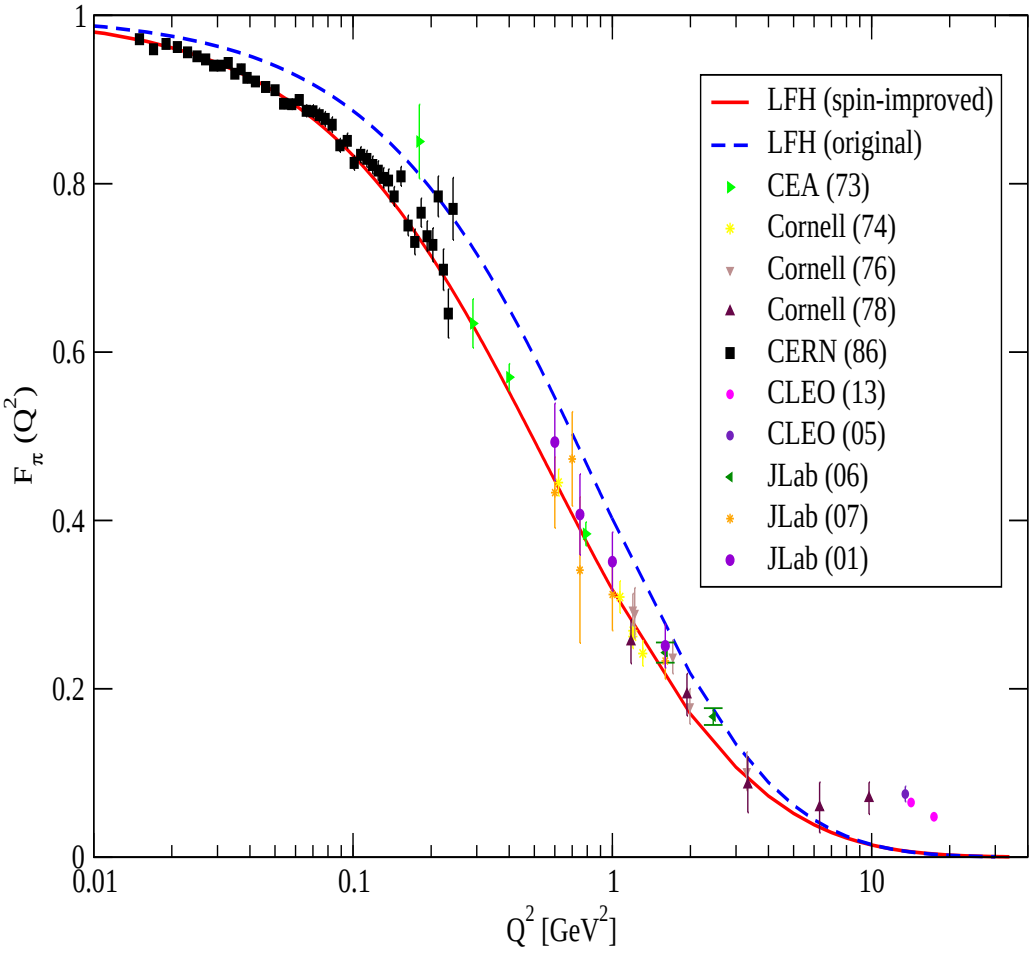

FIG. 3. Our predictions for the pion EM form factor. Continuous-red curve: spin-improved holographic wavefunction. Dashed-blue curve: original holographic wavefunction. Both theory curves generated with $\kappa = 0.523$ GeV and $m_f = 0.330$ GeV. Data from [47, 49–55].

the authors of Ref. [15] imply $P_{q\bar{q}} = 0.62$ in order to fit the decay constant, they implicitly assume $P_{q\bar{q}} = 1$ when computing the EM form factor. This is why we are able to reproduce their prediction for the pion radius even though we assume $P_{q\bar{q}} = 1$.

For completeness, we also compute the transverse size, $R_\perp$, of the pion defined as [43]

$$R_\perp = \frac{1}{\sqrt{\langle k^2 \rangle}} \tag{28}$$

	$\sqrt{\langle r_\pi^2 \rangle}$ [fm]
Original	0.544
Spin-improved	0.683
Experiment [56]	0.672 ± 0.008

TABLE I. Our predictions for the pion radius with $\kappa = 0.523$ GeV and $m_f = 330$ MeV. The datum is from PDG 2014 [56].

	$\sqrt{\langle k^2 \rangle}$ [MeV]	$R_\perp$[fm]
Original	250	0.791
Spin-improved	286	0.690

TABLE II. Our predictions for the mean transverse momentum and size with $\kappa = 0.523$ GeV and $m_f = 330$ MeV.

where

$$\langle k^2 \rangle = \int \mathrm{d}x \mathrm{d}^2\mathbf{k} \mathbf{k}^2 \sum_{h\bar{h}} |\Psi_{h\bar{h}}(x, \mathbf{k})|^2 \tag{29}$$

is the mean value of the quark (or antiquark) transverse momentum squared. Our results are shown in Table II. It can be seen that for both holographic wavefunctions, we predict $\sqrt{\langle k^2 \rangle} \sim m_f > M_\pi$ which, as noted in Ref. [43], confirms the highly relativistic nature of the pion. As expected, our spin-improved holographic wavefunction gives a more reasonable prediction (as expected from the measured radius) for the transverse size of the pion.

IV. DECAY CONSTANT AND DISTRIBUTION AMPLITUDE

The pion decay constant, f_π, is defined by [28]

$$\langle 0|\bar{\Psi}_d \gamma^\mu (1 - \gamma_5) \Psi_u |\pi^+\rangle = i f_\pi P^\mu \, . \tag{30}$$

Taking $\mu = +$ and expanding the left-hand-side of Eq. (30), we obtain

$$\langle 0|\bar{\Psi}_d \gamma^+ (1 - \gamma^5) \Psi_u |\pi^+\rangle = \sqrt{4\pi N_c} \sum_{h,\bar{h}} \int \frac{\mathrm{d}^2\mathbf{k}}{16\pi^3} \mathrm{d}x \Psi^\pi_{h,\bar{h}}(x, \mathbf{k}) \left\{ \frac{\bar{v}_{\bar{h}}}{\sqrt{1-x}} (\gamma^+ (1 - \gamma^5)) \frac{u_h}{\sqrt{x}} \right\} \, . \tag{31}$$

The light-front matrix element in curly brackets can readily be evaluated:

$$\left\{ \frac{\bar{v}_{\bar{h}}}{\sqrt{1-x}} (\gamma^+ (1 - \gamma^5)) \frac{u_h}{\sqrt{x}} \right\} = 2P^+ (1 - h) \delta_{-h\bar{h}} \tag{32}$$

	f_π [MeV]
Original	114
Spin-improved	135
Experiment [56]	$130.4 \pm 0.04 \pm 0.2$

TABLE III. Our predictions for the pion decay constant with $\kappa = 0.523$ GeV and $m_f = 330$ MeV. The datum is from PDG 2014 [56].

which implies that only the opposite-helicities term in the holographic wavefunction contributes to the decay constant. We note, however, that the same-helicities term affects the normalization of our wavefunction and thus our prediction for the decay constant. Using our spin-improved wavefunction, Eq. (20), we deduce that

$$f_\pi = 2\sqrt{\frac{N_c}{\pi}} m_f M_\pi \int dx \frac{\Psi^\pi(x,\zeta)}{x(1-x)}\bigg|_{\zeta=0} . \tag{33}$$

On the other hand, using the original holographic wavefunction, Eq. (21), we obtain

$$f_\pi^{[\mathrm{o}]} = 2\sqrt{6}\sqrt{4\pi} \int \mathrm{d}x \frac{\mathrm{d}^2\mathbf{k}}{16\pi^3} \Psi(x,\mathbf{k}) = 2\sqrt{2}\sqrt{\frac{N_c}{4\pi}} \int dx \Psi^\pi(x,\zeta)\bigg|_{\zeta=0} \tag{34}$$

where we have written the momentum-space expression to point out that, up to a factor of $\sqrt{4\pi}$, it coincides with the formula for the decay constant given in Ref. [57] and widely used in the literature, as for example, in Refs. [15, 27, 58]. The $\sqrt{4\pi}$ factor mismatch is consistent with the fact that our normalization in momentum-space (Eq. (12)) differs from the conventional light-front normalization [28] by a factor of 4π.

Our predictions for the pion decay constant are shown in Table III. As can be seen, we also achieve a much better agreement for this observable with our spin-improved holographic wavefunction, reducing the percentage difference between the theory prediction and the central measured value [56] from 13% to 4%.

We also predict the twist-2 holographic pion DA, $\varphi_\pi(x,\mu)$, defined as [28, 59]

$$\langle 0|\bar{\Psi}_d(z)\gamma^+(1-\gamma_5)\Psi_u(0)|\pi^+\rangle = f_\pi P^+ \int dx e^{ix(P\cdot z)} \varphi_\pi(x,\mu) \tag{35}$$

where $z^2 = 0$. The DA is conventionally normalized as

$$\int dx \varphi(x,\mu) = 1 \tag{36}$$

such that taking the limit of local operators ($z \to 0$) in Eq. (35), we recover the definition of the pion decay constant given by Eq. (30) (with $\mu = +$). Proceeding in the same manner as for the decay constant, we are able to show that

$$f_\pi \varphi_\pi(x,\mu) = 2 m_f M_\pi \sqrt{\frac{N_c}{\pi}} \int \mathrm{d}b J_0(\mu b) b \frac{\Psi(\zeta,x)}{x(1-x)} \tag{37}$$

when using our spin-improved holographic wavefunction, and

$$f_\pi^{[\mathrm{o}]} \varphi_\pi^{[\mathrm{o}]}(x,\mu) = \sqrt{2} \sqrt{\frac{N_c}{\pi}} \int \mathrm{d}b J_0(\mu b) b \Psi(\zeta,x) \; . \tag{38}$$

when using the original holographic wavefunction.

In Figure 4, we compare our spin-improved holographic DA given by Eq. (37) to the original holographic DA given by Eq. (38) and to the asymptotic DA as predicted in pQCD: $\varphi_\pi(x,\infty) = 6x(1-x)$. It can be seen that our spin-improved holographic DA (continuous-red curve) is broader than both the original holographic DA (dashed-blue curve) and the asymptotic DA (dotted-black curve). The holographic DAs are both generated with $\mu = 1$ GeV and we note they hardly evolve for $\mu > 1$ GeV. In other words, our holographic DAs lack the hard, perturbative evolution given by the Efremov-Radyushkin-Brodsky-Lepage (ERBL) equations [60–62]. In Figure 5, we show the soft evolution of our spin-improved holographic DA between $\mu = 0.3$ GeV and $\mu = 1$ GeV. Implementing the ERLB evolution, as is done in Ref. [63], will allow our spin-improved holographic DA to evolve beyond $\mu = 1$ GeV onto the asymptotic DA.

In order to compare our holographic DAs with the predictions of standard non-perturbative methods such as lattice QCD and QCD Sum Rules, we compute the moments defined as

$$\langle \xi_n \rangle = \int_0^1 \mathrm{d}x (2x-1)^n \varphi(x,\mu) \tag{39}$$

and its inverse moment is given by

$$\langle x^{-1} \rangle = \int_0^1 \mathrm{d}x \frac{\varphi(x,\mu)}{x} \; . \tag{40}$$

Our predictions for the first two non-vanishing moments $\langle \xi_2 \rangle$ and $\langle \xi_4 \rangle$ as well as the inverse moment are shown in Table IV. As can be seen, with the spin-improved holographic DA, we achieve better agreement with the predictions of lattice QCD and QCD Sum Rules. However, our predicted moments turn out to be smaller than the predictions of all non-perturbative

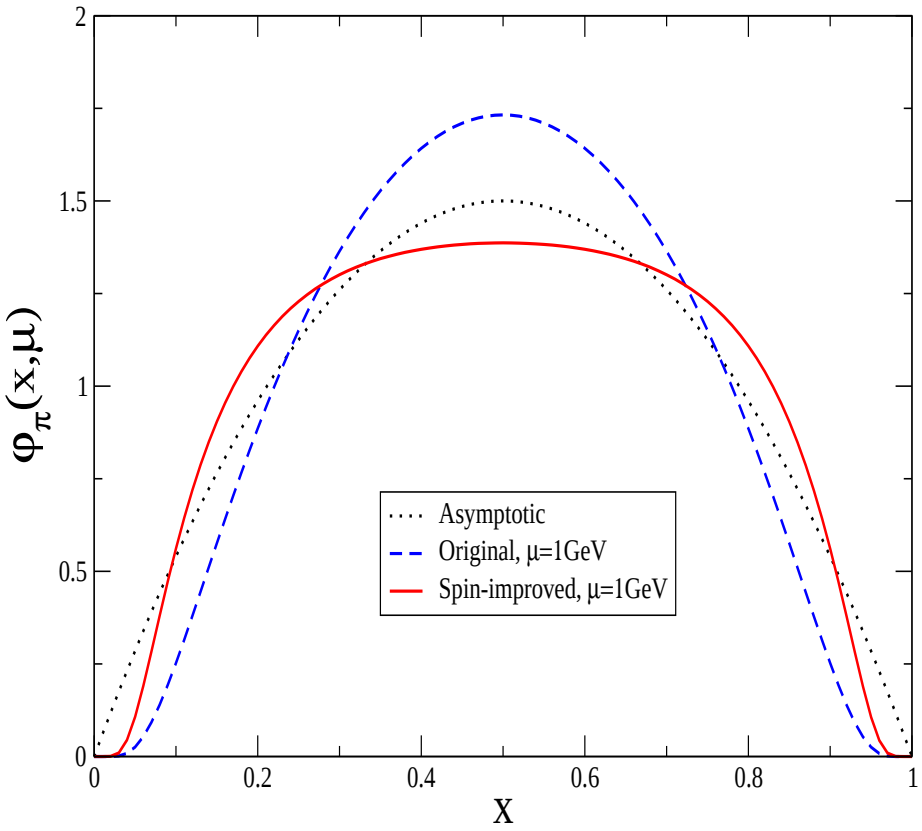

FIG. 4. Comparing our spin-improved holographic DA (continuous-red curve) to the original holographic DA (dashed-blue curve) at a scale $\mu = 1$ GeV, both with $\kappa = 523$ GeV and $m_f = 330$ MeV. The asymptotic DA is the dotted black curve.

methods cited here. Our predicted moments are also smaller than the corresponding moments of the asymptotic DA. This discrepancy could be an indication that all dynamical spin effects are not fully captured by the simple γ^5 ansatz for the spin structure of the pion-$q\bar{q}$ vertex.

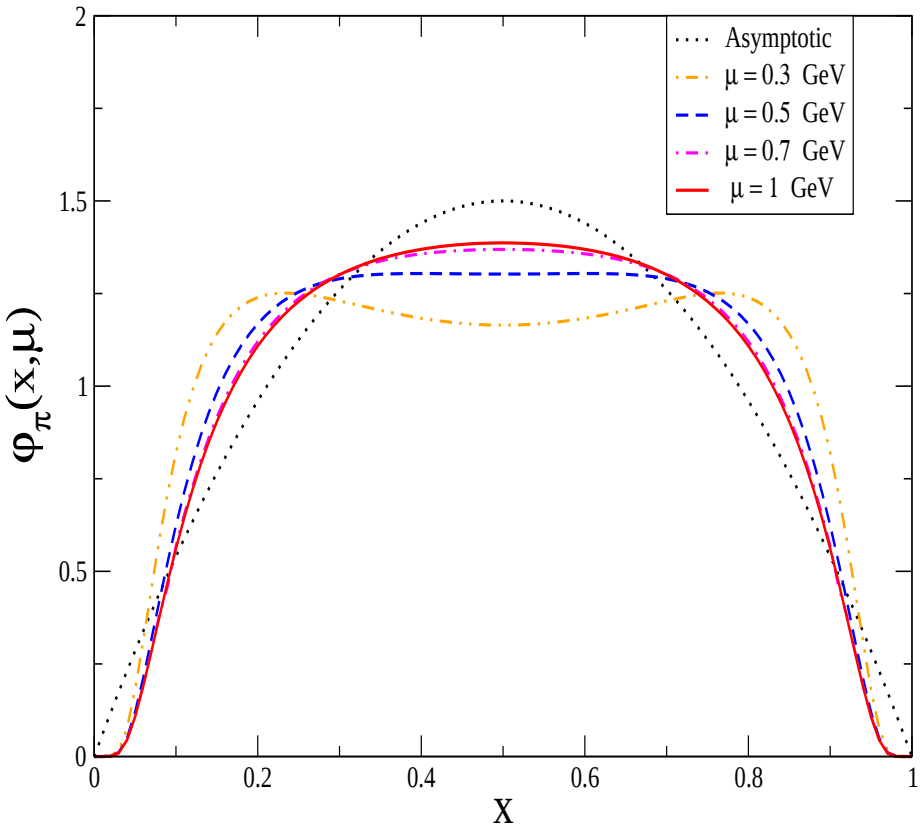

FIG. 5. The soft evolution of our spin-improved holographic pion DA, with $\kappa = 523$ MeV and $m_f = 330$ MeV, at a scale $\mu = 0.3$ GeV(dot-dot-dashed-orange), $\mu = 0.5$ GeV (dashed-blue), $\mu = 0.7$ GeV (dot-dashed-magenta) and $\mu \geq 1$ GeV (continuous-red). The asymptotic DA is the dotted-black curve.

V. PHOTON-TO-PION TRANSITION FORM FACTOR

Using our holographic DAs, we are able to predict the photon-to-pion transition form factor (TFF) which, to leading order in pQCD, is given as [28]

$$F_{\gamma\pi}(Q^2) = \frac{\sqrt{2}}{3} f_\pi \int_0^1 \mathrm{d}x \frac{\varphi_\pi(x, xQ)}{Q^2 x} \,. \tag{41}$$

We note that, even when computing the TFF in the perturbative region $Q^2 \geq 1$ GeV^2, the DA itself is probed at a scale $\mu = xQ$, which can be low if x is close to its end-points. Figure

	μ [GeV]	$\langle\xi_2\rangle$	$\langle\xi_4\rangle$	$\langle x^{-1}\rangle$
Asymptotic	∞	0.2	0.085	3
LFH (spin-improved)	~ 1	0.199	0.078	2.76
LFH (original)	~ 1	0.151	0.050	2.50
LF Quark Model [41]	~ 1	0.24[0.22]	0.11[0.09]	
Sum Rules [64]	1	0.24	0.11	
Renormalon model [65]	1	0.28	0.13	
Instanton vacuum [66, 67]	1	$0.22, 0.21$	$0.10, 0.09$	
Lattice [68, 69]	2	$0.2361(41)(39), 0.27 \pm 0.04$		
NLC Sum Rules [70]	2	$0.248^{+0.016}_{-0.015}$	$0.108^{+0.05}_{-0.03}$	$3.16^{+0.09}_{-0.09}$
Sum Rules[71]	2	0.343	0.181	4.25
Dyson-Schwinger[RL,DB][72]	2	$0.280, 0.251$	$0.151, 0.128$	$5.5, 4.6$

TABLE IV. Our predictions for the first two non-vanishing moments and the inverse moment of the pion holographic twist-2 DA with $\kappa = 523$ MeV and $m_f = 330$ MeV, compared to the predictions of lattice QCD by Braun et al. in 2006 [69] and 2015 [68], QCD Sum Rules with non-local condensates by Bakulaev et al. [70], QCD Sum Rules by Chernyak and Zhitnitsky [71], QCD Sum Rules by Ball and Zwicky [64], light-front quark model of Choi and Ji with two different potentials [41], renormalon model of Agaev [65], instanton vacuum models of Petrov et al. [66] and Nam et al. [67], Dyson-Schwinger Equations of Chang et al. [72] in the rainbow-ladder (RL) approximation and using the dynamical chiral symmetry breaking improved kernel (DB).

6 shows that our spin-improved holographic DA (solid-red curve) does a much better job than the original holographic DA (dashed-blue curve) to describe the available data over the whole Q^2 range. We note that the agreement with data extends to large $Q^2 > 10$ GeV^2 although neither holographic DA can fit the BaBar (2009) data [73]. The BaBar (2009) data indicate a strong scaling violation in disagreement with the Brodsky-Lepage limit: $F_{\pi\gamma^*\gamma}(Q^2 \to \infty) = \sqrt{2} f_\pi$ obtained by substituting the asymptotic DA in Eq. (41) and shown as the dotted-black curves in Figure 6. The more recent Belle (2012) data [74] do not confirm the BaBar (2009) data for $Q^2 > 10$ GeV^2 and the issue is likely to be resolved by precise future measurements in this kinematic range. For alternative models of the pion DA which are able to accommodate the BaBar (2009) data, we refer to Refs. [75–77] and

for an exhaustive analysis of the TFF data, we refer to Ref. [78]. Our predictions with the holographic pion DA clearly cannot describe the BaBar (2009) data and indeed does not overshoot the Brodsky-Lepage limit at asymptotically large Q^2.

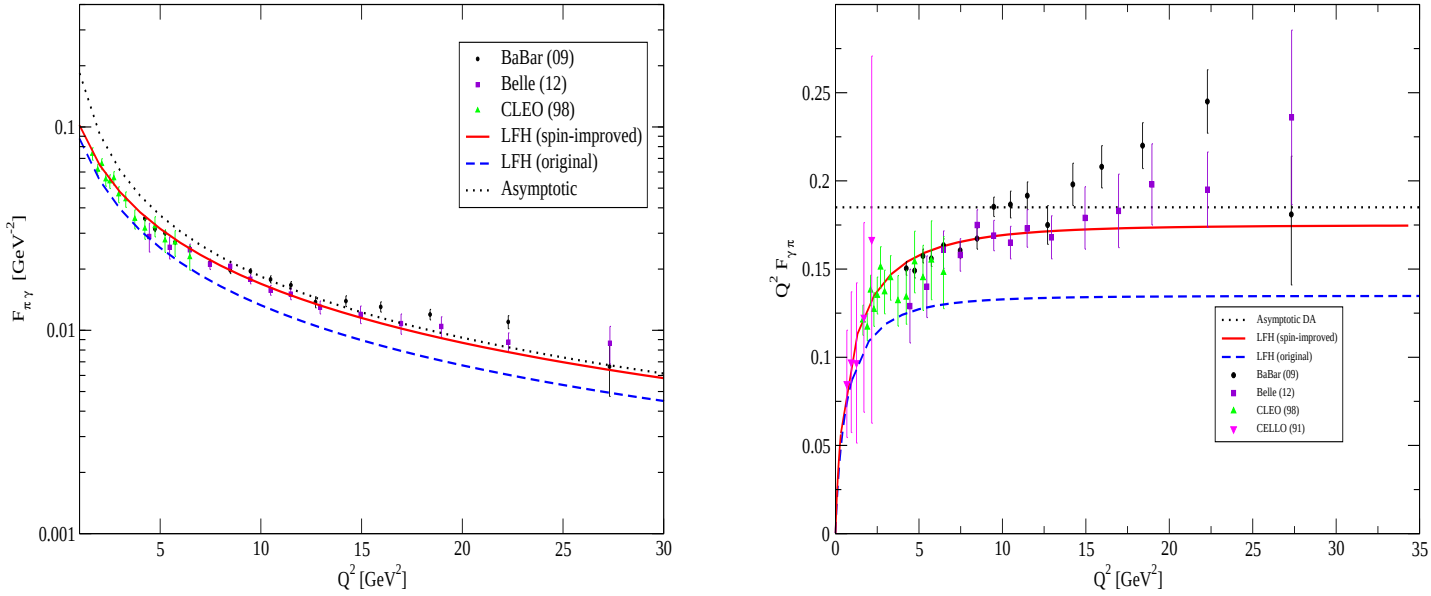

FIG. 6. Our predictions for the photon-to-pion TFF (left) and its scaling behaviour (right) as a function of the photon's virtuality, Q^2. Dashed-blue curve: original holographic DA. Continuous-red curve: spin-improved holographic DA. All theory curves are generated with $\kappa = 523$ MeV and $m_f = 330$ MeV. The dotted black curves are generated using the asymptotic DA with the measured pion decay constant. For asymptotic Q^2, they indicate the Brodsky-Lepage limit. The data are from CELLO [79], CLEO [80], BaBar [74] and Belle [74].

VI. CONCLUSIONS

We have accounted for dynamical quark spin effects in the holographic pion light-front wavefunction and found a remarkable improvement in the description of pion radius, decay constant, EM form factor and photon-to-pion TFF. We have used a universal AdS/QCD scale $\kappa = 523$ MeV and a constituent quark mass of 330 MeV together with the assumption that the pion consists only of the leading quark-antiquark Fock state. Our results suggest

that it is possible to have a unified treatment of all light mesons, including the pion, with a universal fundamental AdS/QCD scale which fits the baryon and meson Regge slopes and also accurately predicts the non-perturbative QCD scale $\Lambda_{\rm QCD}^{\overline{MS}}$. We also found that the predicted moments for the spin-improved holographic pion twist-2 DA are in better agreement with the predictions of standard non-perturbative methods such as lattice QCD and QCD Sum Rules, although they remain smaller than the latter. This suggests that the simple ansatz we use for modelling the dynamical spin effects in the pion, might not be capturing all such effects. It does nevertheless bring a significant improvement in the description of all available experimental data without necessarily having to use a much smaller AdS/QCD scale and/or invoke higher Fock states contributions for the pion. Our findings support the idea of the emergence of a universal AdS/QCD confinement scale κ.

VII. ACKNOWLEDGEMENTS

The work of M.A and R.S is supported by a team grant from National Science and Engineering Research Council of Canada (NSERC). F.C and R.S thank Mount Allison University for hospitality where parts of this work were carried out.

[1] T. Horn and C. D. Roberts, J. Phys. **G43**, 073001 (2016), 1602.04016.

[2] A. Ali, Int. J. Mod. Phys. **A31**, 1630036 (2016), 1607.04918.

[3] S. J. Brodsky, G. F. de Teramond, H. G. Dosch, and J. Erlich, Phys. Rept. **584**, 1 (2015), 1407.8131.

[4] S. J. Brodsky, H.-C. Pauli, and S. S. Pinsky, Phys. Rept. **301**, 299 (1998), hep-ph/9705477.

[5] G. F. de Teramond and S. J. Brodsky, Phys. Rev. Lett. **102**, 081601 (2009), 0809.4899.

[6] S. J. Brodsky and G. F. de Teramond, Phys. Rev. Lett. **96**, 201601 (2006), hep-ph/0602252.

[7] G. F. de Teramond and S. J. Brodsky, Phys. Rev. Lett. **94**, 201601 (2005), hep-th/0501022.

[8] S. J. Brodsky and G. F. de Teramond, Phys. Rev. **D77**, 056007 (2008), 0707.3859.

[9] S. J. Brodsky, G. F. de Téramond, H. G. Dosch, and C. Lorcé, Int. J. Mod. Phys. **A31**, 1630029 (2016), 1606.04638.

[10] S. J. Brodsky, G. F. De Téramond, and H. G. Dosch, Phys. Lett. **B729**, 3 (2014), 1302.4105.

[11] S. J. Brodsky, G. F. de Téramond, and H. G. Dosch, Nuovo Cim. **C036**, 265 (2013), 1302.5399.

[12] V. de Alfaro, S. Fubini, and G. Furlan, Nuovo Cim. **A34**, 569 (1976).

[13] S. J. Brodsky and G. F. de Teramond, Phys. Rev. **D78**, 025032 (2008), 0804.0452.

[14] S. D. Glazek and A. P. Trawiński, Phys. Rev. **D88**, 105025 (2013), 1307.2059.

[15] R. Swarnkar and D. Chakrabarti, Phys. Rev. **D92**, 074023 (2015), 1507.01568.

[16] S. J. Brodsky and G. F. de Teramond, Subnucl. Ser. **45**, 139 (2009), 0802.0514.

[17] S. J. Brodsky, G. F. de Teramond, and A. Deur, Phys. Rev. **D81**, 096010 (2010), 1002.3948.

[18] A. Deur, S. J. Brodsky, and G. F. de Teramond (2016), 1608.04933.

[19] J. R. Forshaw and R. Sandapen, Phys. Rev. Lett. **109**, 081601 (2012), 1203.6088.

[20] M. Ahmady, R. Sandapen, and N. Sharma (2016), 1605.07665.

[21] R. S. Sufian, G. F. de Téramond, S. J. Brodsky, A. Deur, and H. G. Dosch (2016), 1609.06688.

[22] S. J. Brodsky, F.-G. Cao, and G. F. de Teramond, Phys. Rev. **D84**, 075012 (2011), 1105.3999.

[23] S. D. Drell and T.-M. Yan, Phys. Rev. Lett. **24**, 181 (1970).

[24] G. B. West, Phys. Rev. Lett. **24**, 1206 (1970).

[25] A. Vega and I. Schmidt, Phys. Rev. **D79**, 055003 (2009), 0811.4638.

[26] A. Vega, I. Schmidt, T. Branz, T. Gutsche, and V. E. Lyubovitskij, Phys. Rev. **D80**, 055014 (2009), 0906.1220.

[27] T. Branz, T. Gutsche, V. E. Lyubovitskij, I. Schmidt, and A. Vega, Phys. Rev. **D82**, 074022 (2010), 1008.0268.

[28] G. P. Lepage and S. J. Brodsky, Phys. Rev. **D22**, 2157 (1980).

[29] H. G. Dosch, T. Gousset, G. Kulzinger, and H. J. Pirner, Phys. Rev. **D55**, 2602 (1997), hep-ph/9608203.

[30] G. Kulzinger, H. G. Dosch, and H. J. Pirner, Eur. Phys. J. **C7**, 73 (1999), hep-ph/9806352.

[31] J. Nemchik, N. N. Nikolaev, E. Predazzi, and B. G. Zakharov, Z. Phys. **C75**, 71 (1997), hep-ph/9605231.

[32] J. R. Forshaw, R. Sandapen, and G. Shaw, Phys. Rev. **D69**, 094013 (2004), hep-ph/0312172.

[33] G. Watt and H. Kowalski, Phys. Rev. **D78**, 014016 (2008), 0712.2670.

[34] J. R. Forshaw, R. Sandapen, and G. Shaw, JHEP **11**, 025 (2006), hep-ph/0608161.

[35] J. R. Forshaw and R. Sandapen, JHEP **11**, 037 (2010), 1007.1990.

[36] J. R. Forshaw and R. Sandapen, JHEP **10**, 093 (2011), 1104.4753.

[37] N. Armesto and A. H. Rezaeian, Phys. Rev. **D90**, 054003 (2014), 1402.4831.

[38] A. H. Rezaeian and I. Schmidt, Phys. Rev. **D88**, 074016 (2013), 1307.0825.

[39] V. P. Goncalves, F. S. Navarra, and D. Spiering, J. Phys. **G43**, 095002 (2016), 1510.01512.

[40] A. H. Rezaeian, M. Siddikov, M. Van de Klundert, and R. Venugopalan, Phys. Rev. **D87**, 034002 (2013), 1212.2974.

[41] H.-M. Choi and C.-R. Ji, Phys. Rev. **D75**, 034019 (2007), hep-ph/0701177.

[42] A. P. Trawiński, Few Body Syst. **57**, 449 (2016).

[43] T. Heinzl, Lect. Notes Phys. **572**, 55 (2001), hep-th/0008096.

[44] T. Heinzl, Nucl. Phys. Proc. Suppl. **90**, 83 (2000), [,231(2000)], hep-ph/0008314.

[45] H. Leutwyler, Nucl. Phys. **B76**, 413 (1974).

[46] H. Leutwyler, Phys. Lett. **B48**, 45 (1974).

[47] S. R. A. *et al* (NA7 collaboration), Nucl. Phys. **B277**, 168 (1986).

[48] C. N. B. *et al*, Phys. Rev. **D8**, 92 (1973).

[49] C. J. B. *et al*, Phys. Rev. **D9**, 1229 (1974).

[50] C. J. B. *et al*, Phys. Rev. **D13**, 25 (1976).

[51] C. J. B. *et al*, Phys. Rev. **D17**, 1693 (1978).

[52] J. V. *et al* (The Jefferson Lab Fπ Collaboration), Phys. Rev. Lett. **86**, 1713 (2001), hep-ph/0602252.

[53] T. H. *et al* (The Jefferson Lab Fπ Collaboration), Phys. Rev. Lett. **97**, 192001 (2006), nucl-ex/0607005.

[54] T. K. P. *et al* (CLEO collaboration), Phys. Rev. Lett. **95**, 261803 (2005), hep-ex/0510005.

[55] K. K. Seth, S. Dobbs, Z. Metreveli, A. Tomaradze, T. Xiao, and G. Bonvicini, Phys. Rev. Lett. **110**, 022002 (2013), 1210.1596.

[56] K. A. Olive et al. (Particle Data Group), Chin. Phys. **C38**, 090001 (2014).

[57] G. P. Lepage, S. J. Brodsky, T. Huang, and P. B. Mackenzie, in *Particles and Fields 2. Proceedings, Summer Institute, BANFF, Canada, August 16-27, 1981* (1982), pp. 83–141, URL `http://lss.fnal.gov/archive/preprint/fermilab-conf-81-114-t.shtml`.

[58] S. S. Chabysheva and J. R. Hiller, Annals Phys. **337**, 143 (2013), 1207.7128.

[59] A. V. Radyushkin, Submitted to: Phys. Lett. (1977), hep-ph/0410276.

[60] G. P. Lepage and S. J. Brodsky, Phys. Lett. **B87**, 359 (1979).

[61] A. V. Efremov and A. V. Radyushkin, Theor. Math. Phys. **42**, 97 (1980), [Teor. Mat. Fiz.42,147(1980)].

[62] A. V. Efremov and A. V. Radyushkin, Phys. Lett. **B94**, 245 (1980).

[63] S. J. Brodsky, F.-G. Cao, and G. F. de Teramond, Phys. Rev. **D84**, 033001 (2011), 1104.3364.

[64] P. Ball and R. Zwicky, Phys. Rev. **D71**, 014015 (2005), hep-ph/0406232.

[65] S. S. Agaev, Phys. Rev. **D72**, 114010 (2005), [Erratum: Phys. Rev.D73,059902(2006)], hep-ph/0511192.

[66] V. Yu. Petrov, M. V. Polyakov, R. Ruskov, C. Weiss, and K. Goeke, Phys. Rev. **D59**, 114018 (1999), hep-ph/9807229.

[67] S.-i. Nam, H.-C. Kim, A. Hosaka, and M. M. Musakhanov, Phys. Rev. **D74**, 014019 (2006), hep-ph/0605259.

[68] V. M. Braun, S. Collins, M. Göckeler, P. Pérez-Rubio, A. Schäfer, R. W. Schiel, and A. Sternbeck, Phys. Rev. **D92**, 014504 (2015), 1503.03656.

[69] V. M. Braun et al., Phys. Rev. **D74**, 074501 (2006), hep-lat/0606012.

[70] A. P. Bakulev, S. V. Mikhailov, and N. G. Stefanis, Phys. Lett. **B508**, 279 (2001), [Erratum: Phys. Lett.B590,309(2004)], hep-ph/0103119.

[71] V. L. Chernyak and A. R. Zhitnitsky, Phys. Rept. **112**, 173 (1984).

[72] L. Chang, I. C. Cloet, J. J. Cobos-Martinez, C. D. Roberts, S. M. Schmidt, and P. C. Tandy, Phys. Rev. Lett. **110**, 132001 (2013), 1301.0324.

[73] B. A. *et al* (BaBar collaboration), Phys. Rev. **D80**, 052002 (2009), 0905.4778.

[74] S. U. *et al* (Belle collaboration), Phys. Rev. **D86**, 092007 (2012), 1205.3249.

[75] A. V. Radyushkin, Phys. Rev. **D80**, 094009 (2009), 0906.0323.

[76] M. V. Polyakov, JETP Lett. **90**, 228 (2009), 0906.0538.

[77] H.-n. Li and S. Mishima, Phys. Rev. **D80**, 074024 (2009), 0907.0166.

[78] A. P. Bakulev, S. V. Mikhailov, A. V. Pimikov, and N. G. Stefanis, Phys. Rev. **D86**, 031501 (2012), 1205.3770.

[79] H. J. B. *et al* (CELLO collaboration), Z. Phys. **C49**, 401 (1991).

[80] J. G. et al (CLEO collaboration), Phys. Rev. **D57**, 33 (1998), hep-ex/9707031.